


Optically induced magnetization reversal in [Co/Pt]_N multilayers: Role of domain wall dynamicsU. Parlak,^{*} R. Adam,[†] D. E. Bürgler, S. Gang, and C. M. Schneider*Peter Grünberg Institut, Research Centre Jülich, 52425 Jülich, Germany* (Received 27 September 2018; revised manuscript received 5 December 2018; published 27 December 2018)

All-optical switching (AOS) of magnetization in ferri- and ferromagnetic thin films has in recent years attracted a strong interest since it allows magnetization reversal in the absence of applied magnetic field. Here we investigate AOS in [Co/Pt]_N multilayers. The coercivity (H_C) of the multilayers was tuned either by varying the bilayer repetition number (N) or the sample temperature (T). During the AOS experiments, we first illuminated the multilayers by a sequence of femtosecond laser pulses with varying fluence, light polarization, and repetition rate. The optically affected area was then imaged with magneto-optical Kerr microscopy. Our results indicate that the optical pulses can trigger either AOS or initiate an all-optical domain formation (AODF). The laser fluence required for AOS scales linearly with H_C and depends on a precise tuning of laser pulse fluence, repetition rate, and light polarization. Furthermore, the magnetic response of the samples at a varying ambient temperature (down to 50 K) and for different time intervals between subsequent laser pulses point to the crucial role of domain wall dynamics in optical control of magnetization in ferromagnetic multilayers.

DOI: [10.1103/PhysRevB.98.214443](https://doi.org/10.1103/PhysRevB.98.214443)**I. INTRODUCTION**

Interaction of ultrafast laser pulses with magnetic materials has been under intense investigation since the pioneering experimental work of Beaurepaire *et al.* [1]. This and the further experiments revealed that the illumination of magnetic thin films with laser pulses results in a magnetization quenching that occurs on a femtosecond timescale with a subsequent recovery within picoseconds [2–4]. In 2007 Stanciu *et al.* experimentally showed that circularly polarized femtosecond pulses can be applied to deterministically alter the magnetization state of ferrimagnetic GdFeCo films depending on the laser helicity [5]. In the subsequent studies, all-optical *helicity-dependent* switching (AO-HDS) has been observed in a number of rare earth-transition metal alloys, multilayers, and synthetic ferrimagnets [6–8]. In addition, the alloy composition and structure were found to strongly affect the response of a ferrimagnetic material to the laser pulses [9]. All-optical *helicity-independent* switching (AO-HIS) was theoretically predicted and experimentally demonstrated too, notably in similar GdFeCo alloys, but using linearly polarized single pulses contrary to AO-HDS [10,11]. The analysis of the results shows that the AO-HDS and AO-HIS mechanisms differ. While the mechanism of AO-HDS in ferrimagnetic materials is still under debate [12], AO-HIS is a heat driven process attributed to a transient ferromagnetic state arising as a consequence of different demagnetization times of the antiparallel oriented Fe and Gd spin sublattices [10]. On the other hand, in ferromagnetic materials, all spins point in the same direction and, contrary to ferrimagnets, there are no antiparallel sublattices present. Therefore, the demonstration of the all-optical switching (AOS) in *ferromagnetic multilayers*

by Lambert *et al.* [13] raised many questions about the possible underlying physical mechanism. Up to date, AOS has been observed only in a limited number of ferromagnetic multilayers and granular media [13–15]. Due to the fact that AOS is only shown in a class of materials that includes interfaces [8] or chemical inhomogeneities [15], it has been proposed that interlayer exchange interactions and spin-orbit coupling contribute to the effect [16]. The mechanism of AOS in ferromagnetic materials has been investigated theoretically [17,18] and experimentally [19,20] by a number of groups. The ongoing discussion suggests that, similar to the case of ferrimagnets, AOS is based on a combination of the laser-induced heating, magnetic circular dichroism (MCD) [17,21,22], and inverse Faraday effects (IFE) [18,23–25]. Concerning the role of MCD, one can assume that different magnetically oriented domains absorb different amounts of energy during laser illumination depending on the relative direction of local magnetization and helicity of the incoming laser beam [21]. As a result, domains with opposite magnetization can heat up differently, which leads to a difference in the rate of reversal between the two states of magnetization directions due to the Boltzmann factor ($\Delta E/k_B T$). Consequently, one magnetic domain state (“up” or “down” magnetized) becomes less stable than the other. This area is then more susceptible to demagnetization or magnetization reversal which proceeds stochastically by thermally driven hopping processes. Similarly, the magnetic field due to IFE is also considered to be a symmetry breaking factor in AOS [26]. Nevertheless, the questions about the strength of optically induced IFE magnetic field as well as material and wavelength dependencies are still under debate.

Contrary to ferrimagnetic films, up to now, there have been only a few publications reporting single-pulse-triggered AOS in ferromagnetic films [27–29]. Gorchon *et al.* reported single-pulse switching of Co/Pt multilayers when the multilayers are coupled to a GdFeCo ferrimagnetic alloy [28] indicating that

^{*}u.parlak@fz-juelich.de[†]r.adam@fz-juelich.de

an inclusion of a ferrimagnetic layer may be necessary for single-pulse switching. Lalieu *et al.* demonstrated single-pulse switching of Pt/Co/Gd stacks with linearly polarized pulses [27]. Recently, Vomir *et al.* reported helicity-independent single-pulse switching in Pt/Co/Pt stacks by reducing the beam spot diameter down to the size of intrinsic domains [29]. Except from these reports, *single-pulse* laser illumination of [Co/Pt] $_N$ ferromagnetic multilayers has been reported to reveal all-optical domain formation (AODF), i.e., a breakdown of the magnetization into randomly distributed domains, regardless of the beam polarization [17,20].

In this study we fabricated a set of [Co/Pt] $_N$ multilayers with different bilayer repetition numbers for which magneto-optical Kerr effect (MOKE) magnetometry in the temperature range from 300 down to 50 K reveals an increasing coercivity (H_C) both with increasing N and a decreasing temperature T . Therefore, these samples allowed us to explore the relationship between coercivity of the multilayers and their response to the illumination by femtosecond laser pulses. In addition, we observed appreciable variations in the size of the optically affected area by tuning the time interval between the pulses.

II. EXPERIMENTAL DETAILS

We fabricated [Co(0.4 nm)/Pt(0.7 nm)] $_N$ multilayers on top of oxidized Si(001) wafers by magnetron sputtering at room temperature. $N = 3, 5, 7,$ and 9 represents the Co/Pt bilayer repetition number. The deposition rate for each material was monitored by a quartz crystal microbalance that was calibrated by x-ray reflectivity (XRR) measurements. XRR was also used to verify the thickness of the multilayer stack after the fabrication process. A buffer layer of Ta (5 nm) was deposited prior to multilayer growth in order to achieve a good interface smoothness required for strong perpendicular magnetic anisotropy (PMA) [30]. A Pt capping layer (2 nm) was deposited on top of the multilayer to prevent surface oxidation. In order to confirm out-of-plane magnetization, static MOKE magnetometry was employed in polar geometry for measuring the magnetic hysteresis loops of the multilayers. In order to optically control the magnetization orientation, we used a Ti:sapphire laser amplifier system (Spitfire Pro from Spectra-Physics) generating a train of pulses with approximately 70 fs pulse duration and 800 nm central wavelength. The amplifier controller allowed an adjustable pulse repetition rate from 20 Hz to 1 kHz, with the additional option of manual triggering to generate single pulses. A half-wave plate (HWP) in combination with a Glan-Thompson linear polarizer prism was used to provide linearly polarized light with adjustable intensity. A quarter-wave plate (QWP) was introduced to transform the linear polarization of the light into circular polarization. “Left” or “right” circular polarization of the beam was adjusted by rotating the QWP by $\pm 45^\circ$ with respect to the plane of linear polarization. The laser beam with a Gaussian profile was focused to the sample using a $10\times$ plan-apochromat objective (Mitutoyo) with a numerical aperture of 0.28. The Gaussian shape was confirmed with knife-edge scans across the beam profile. In all experiments the $1/e^2$ beam spot size was $100 \pm 5 \mu\text{m}$ at the sample position. The sample was mounted on a microstep motor-controlled linear

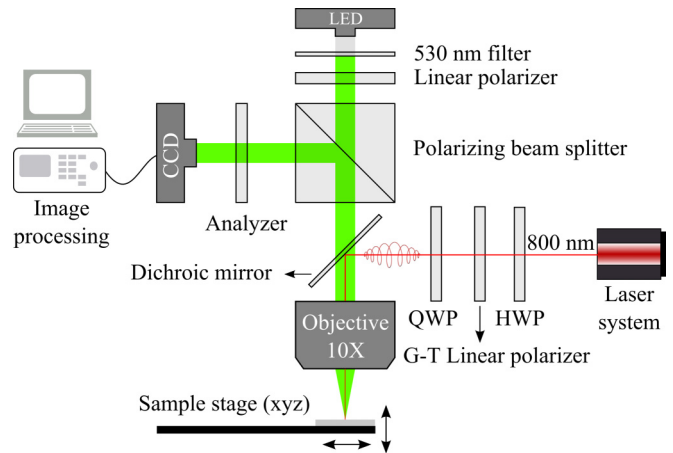


FIG. 1. A magneto-optical Kerr microscopy with polar sensitivity was coupled to the femtosecond laser system using a dichroic mirror. A light-emitting diode (LED) served as a light source for the Kerr microscope. The white LED beam was filtered at 530 nm for maximizing the Kerr rotation. The reflected imaging beam was directed towards the charge-coupled-device (CCD) camera by a polarizing beam splitter. Magnetic contrast was detected by polarization analyzer. While imaging the magnetic domains, the laser beam was focused on the sample through the same objective lens to induce a magnetization state. We controlled the laser fluence using the combination of a Glan-Thompson (G-T) linear polarizer and half-wave plate (HWP), and the polarization state was controlled by the quarter-wave plate (QWP). In AOS experiments, the laser wavelength and pulse duration were fixed at $\lambda = 800 \text{ nm}$ and $\tau \sim 70 \text{ fs}$, respectively.

stage, which allows one to tune the number of pulses per illuminated area by varying the stage velocity.

For the imaging of the magnetic domain state after laser illumination, we combined a magneto-optical Kerr microscope with a lateral resolution of approximately $5 \mu\text{m}$ with a femtosecond laser system as shown in Fig. 1. A white light-emitting diode (LED) beam, used for imaging, was guided through a 530 nm glass filter in order to separate the wavelengths of the excitation and the imaging beams and to maximize the Kerr rotation [31]. The reflected beam was directed towards the charge-coupled-device (CCD) camera and the magnetic contrast was obtained using the polarization analyzer. In most of the experiments, we induced a magnetic domain wall using a permanent magnet prior to the exposure to laser pulses. The optically induced modifications in the domain structure were imaged first. After the magnetic image was taken, the sample was saturated by the external magnetic field to obtain the background image of the single domain state. The image of the optically induced, nonsaturated state was then divided by the background image to enhance the magnetic contrast. The effects of uneven illumination were corrected by polynomial background correction.

Low-temperature experiments were carried out in a Helium-flow optical cryostat (Oxford Instruments) capable of reaching temperatures down to 10 K. The window of the cryostat did not introduce measurable depolarization effects. The sample was mounted on a copper cold finger and the

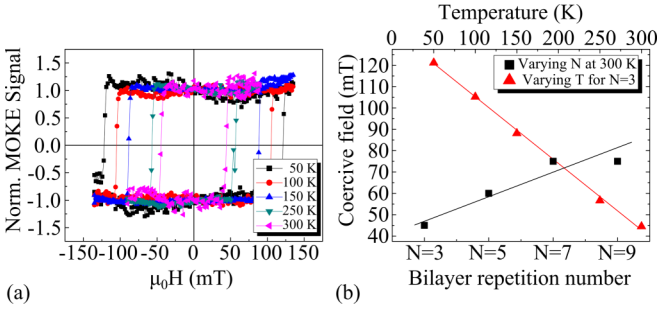


FIG. 2. (a) Magnetic hysteresis loops of the $[\text{Co/Pt}]_3$ sample at temperatures between 50 and 300 K show PMA and 100% remanence at all temperatures. (b) Coercive fields of multilayers with varying N measured at 300 K (black squares and lower abscissa) and for $[\text{Co/Pt}]_3$ measured at varying T (red triangles and upper abscissa). The full lines are guides for the eye.

experiments were performed in a temperature range of 300–50 K.

III. RESULTS AND DISCUSSION

A. Magnetic properties of $[\text{Co/Pt}]_N$ multilayers

Prior to the AOS experiments, we performed a magnetic characterization of the $[\text{Co/Pt}]_N$ multilayers. Magnetic hysteresis loops of the multilayers with varying T and N were measured. The measurements indicate PMA with 100% remanent magnetization for all multilayer stacks which has been suggested to be a prerequisite for AOS [32]. Furthermore, a strong PMA enhances the magnetic contrast in the magneto-optic imaging and maintains a stable domain state. A set of magnetic hysteresis loops for $N = 3$ in the temperature range between $T = 300$ and 50 K is shown in Fig. 2(a). The

measurements confirm that the PMA and the full remanence are sustained at lower temperatures. In addition, the coercive field (H_C) increases by almost a factor of 3 when the temperature reached 50 K as displayed in Fig. 2(b) by red triangles. This effect can be attributed to more efficient domain wall pinning at low temperatures [33]. Figure 2(b) also shows that H_C of the multilayers increases as a function of N (black squares). This observed tendency is attributed to an enhanced coupling between layers [34,35].

B. Quasistatic all-optical switching

Earlier experiments showed that a homogeneously magnetized film can break into a set of randomly distributed domains when exposed to a large optically induced thermal load [13,20,21]. In our experiments, in order to avoid overheating, we only very gradually increased the laser fluence until we observed domain formation. In Figs. 3(a)–3(c) we show the domain state of the $[\text{Co/Pt}]_3$ multilayer after illumination with laser light of three different laser fluence levels. The sample was mounted on the linear translation stage and was horizontally moved with the lowest possible velocity ($1 \mu\text{m/s}$). Figures 3(a)–3(c) show also the light polarization-dependent response for left circularly (σ^-), right circularly (σ^+), and linearly (π) polarized light in the same field of view. Examination of the magnetic contrast reveals two types of magnetic responses of the illuminated area: (i) all-optical domain formation (AODF), denoting the formation of random distributions of domains; and (ii) all-optical switching (AOS), meaning the complete magnetization reversal of the illuminated area. Detailed analysis of the images shows that no magnetization tilt is induced in the illuminated area, which is also confirmed by x-ray photoemission electron microscopy (see Supplemental Material, Fig. 1 [36]).

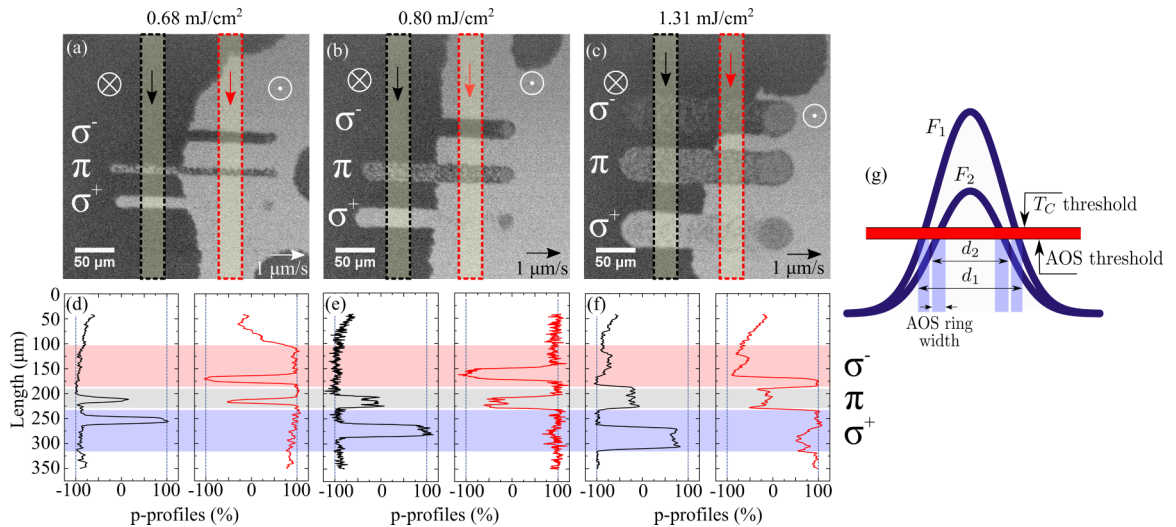


FIG. 3. Laser fluence dependence of AOS in a $[\text{Co/Pt}]_3$ multilayer. Kerr microscopy images show laser illuminated areas after inducing AOS/AODF with a laser fluence of (a) 0.68 mJ/cm^2 , (b) 0.80 mJ/cm^2 , and (c) 1.31 mJ/cm^2 . Profiles of the normalized domain contrast p (see text) are given in (d)–(f) for areas marked by dashed rectangles in the corresponding Kerr microscopy images (a)–(c). The relative positions of σ^+ , π , and σ^- polarized light are depicted by blue, gray, and red backgrounds, respectively. (g) 2D schematics of Gaussian laser intensity profiles for two different fluences F_1 and F_2 that gives rise to AOS only in ringlike areas (light blue), where the local laser fluence is between upper (T_C) and lower (AOS) thresholds (red line).

Magnetic domains with sizes comparable to the resolution of magneto-optical images appear in a gray color depending on the up and down domain concentrations. In order to quantify the optically induced magnetic domain state, we defined the normalized domain contrast parameter p , which ranges between bright and dark colors associated with the saturated domain states. The normalized domain contrast averaged over a certain illuminated area is determined by the fractions of up and down domains f_{\uparrow} and f_{\downarrow} , respectively, where $f_{\uparrow} + f_{\downarrow} = 1$. Accordingly, the averaged net magnetization pointing perpendicular to the film plane is proportional to $p = (f_{\uparrow} - f_{\downarrow}) \times 100$. The p profiles in Figs. 3(d)–3(f) have been measured within the areas of the dashed rectangles shown in Figs. 3(a)–3(c). The p value is defined by horizontal binning of pixel intensities within the defined rectangles, and the p profiles are plotted along the black and red arrows.

Comparing the p profiles of the laser illuminated lines with the reference bright and dark levels of homogeneously magnetized areas, we observe that the [Co/Pt]₃ multilayer exhibits a full AO-HDS at 0.68 and 0.80 mJ/cm² laser fluences. At an increased laser fluence of 1.31 mJ/cm², the analysis shows a helicity-dependent AODF with the normalized domain contrast, p values, close to $\pm 75\%$ for both left and right circularly polarized light. On the other hand, linearly polarized light results in $p \approx 0\%$ for all tested laser fluences. Below the laser fluence of 0.68 mJ/cm², we observed neither AOS nor AODF (no domain formation). These results confirm earlier reported observations that a certain optimum heating in connection with helicity is necessary in order to observe AOS [13,37]. On the other hand, AODF is observed when the upper (T_C) threshold of optimum heating level is exceeded or when illuminated with linearly polarized light. We note that at the end of the lines in Figs. 3(a)–3(c), the AODF regions are often surrounded by a ringlike AOS region, thus indirectly confirming the existence of the laser intensity optimum for AOS.

As noted in the Introduction, AOS in ferromagnetic thin films require multiple laser pulses. To elucidate the effect of pulse accumulation on AOS and AODF in more detail, we illuminated a chosen spot at the sample surface without scanning. In this experiment (see Fig. 4) we defined the number of pulses impinging at the sample by opening a beam shutter for a defined period of time. Only the single pulse illumination was done with the help of the translation stage by increasing its speed to 50 mm/s such that there is no spatial overlap between the consecutive pulses. We started the illumination with a low laser fluence of 0.80 mJ/cm², where single pulses resulted in no observable effects inside the red dashed rectangle in Fig. 4(a). For an increased laser fluence of 1.31 mJ/cm², single pulses result in AODF regardless of the beam polarization, as shown in the first two rows of spots in Fig. 4(b). Further accumulation of pulses ($\geq 10^3$) in both laser fluence levels resulted in (i) AODF at the center of the spot, (ii) an increase of the spot diameter, and (iii) the formation of the completely magnetically switched “AOS ring” at the perimeter of an illuminated spot. The evolution of radial intensity profile with respect to an increasing number of pulses is shown in Figs. 4(c) and 4(d).

Together with the observations presented in Fig. 3, this points to the fact that while AODF can be induced even by

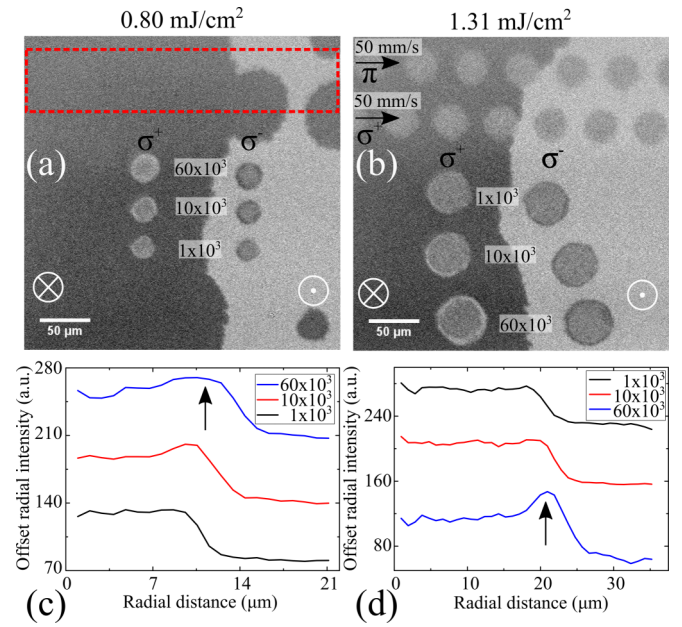


FIG. 4. Kerr microscopy images of the [Co/Pt]₃ multilayer after laser illumination. The dashed rectangle in (a) depicts the area illuminated by the single pulses with a fluence of 0.80 mJ/cm² with no observable AOS or AODF. The effect of single pulses is not observed by optical imaging. Below this area we illuminated the sample with a static beam with 1 kHz repetition rate for varying time durations. Right (σ^+) and left (σ^-) circularly polarized light was exposed to down and up background domains, respectively. (b) The same approach with 1.31 mJ/cm² laser fluence. The first two rows from the top show AODF as a result of single-pulse illumination, regardless of polarization. (c) and (d) The radial intensity profiles of the corresponding spots. Profiles are vertically offset for clarity and arrows mark the fully switched ringlike area at the perimeter of the illuminated spot. Note that the three larger round domains (top right) and one smaller domain (bottom right) are not optically induced domains. They are the background domains induced by a static external magnetic field.

a single pulse above a certain fluence level, AOS always requires multiple laser pulses and only occurs in a narrow range of laser fluences. We stress that while in the experiment shown in Fig. 3, the broadening of the optically modified magnetic line was associated with $1/e^2$ diameter broadening of the laser pulses that scales with the increasing *laser fluence*, in the latter experiment shown in Fig. 4, the broadening of the laser illuminated area scales with the *number of pulses*. This is especially evident at a laser fluence of 0.80 mJ/cm², where the area of the AODF spot size increases 1.25 times between 10^3 and 6×10^4 pulses. Because the laser fluence is the same for every illuminated position, the effect can be ascribed to a *radial heat propagation* around the illuminated spot.

A natural question to ask at this point is which parameters actually determine the “optimum” fluence interval at which AOS occurs. To expand our insight we varied coercivity (H_C) of our [Co/Pt]_N samples by varying bilayer repetition N (as described in Sec. II) and again looked for the optimum laser fluence for AOS. First, a [Co/Pt]₃ sample was illuminated with the fluence (0.82 mJ/cm²) already known to be able to switch this sample [see Fig. 5(a)]. Then we kept the

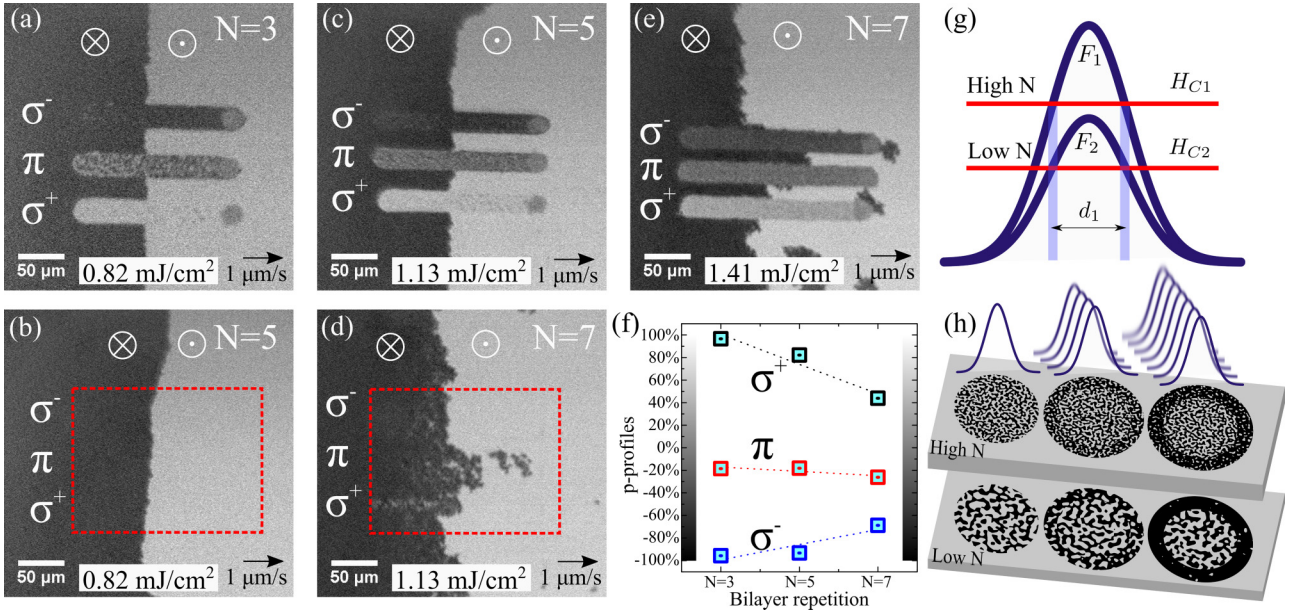


FIG. 5. Kerr microscopy images of $[\text{Co/Pt}]_N$ multilayers for (a) $N = 3$, (b) and (c) $N = 5$, and (d) and (e) $N = 7$. For every N , laser fluence was tuned in order to reach the minimum level F_{\min} required to achieve AODF. Dashed red rectangles in (b) and (d) depict the laser illuminated areas for $N = 5$ and 7 , where the fluence level F_{\min} determined for $N = 3$ and 5 , respectively, is not sufficient to affect the magnetization. (f) Normalized domain contrast p as a function of N and beam polarization calculated from the intensity profiles shown in the Supplemental Material [36]. Dotted lines are guides for the eyes. The error bars are inside the squares. (g) 2D schematics of Gaussian intensity profiles (dark blue) for different laser fluences that resulted in the same linewidth (light blue) in multilayers with different N . This is attributed to the thresholds (red lines) determined by H_C of multilayers. (h) Schematics of domain sizes in multilayers with high N (upper row) and low N (lower row). We illustrate the preferential growth of black domains as a function of the circularly polarized laser pulses (from left to right). Domain growth takes place at the perimeter where optimum AOS fluence is met.

fluence constant and illuminated the $[\text{Co/Pt}]_5$ multilayers. As Fig. 5(b) shows, this fluence turned out to be insufficient to induce either AODF or AOS. In order to induce AODF/AOS in the $[\text{Co/Pt}]_5$ sample, the fluence had to be increased by ~ 0.3 mJ/cm², i.e., by more than 30% [Fig. 5(c)]. For the multilayer with $N = 7$ the fluence must be increased by yet another ~ 0.3 mJ/cm² to achieve AODF [Figs. 5(d) and 5(e)]. In order to elucidate the relation between coercive fields H_C and the minimum fluence F_{\min} required for the onset of AODF, we calculated the ratio F_{\min}/H_C that turns out to be almost the same for all samples, $F_{\min}/H_C \sim 0.018$ mJ cm⁻² mT⁻¹, thus revealing the important role of H_C in determining F_{\min} . We note that in the latter experiment, the increased laser fluence did not result in the line broadening similar to the one shown in Fig. 3 even though an increase of the laser fluence by $\sim 72\%$ was necessary to induce AODF in the sample with $N = 7$ compared to $N = 3$. In all these experiments, the laser fluence was increased very slowly in steps of only 0.05 mJ/cm² in order to identify the minimum fluence F_{\min} affecting the particular sample.

Figure 5(f) shows the p values calculated from the scans along the illuminated lines, see the Supplemental Material, Fig. 2 [36]. In this analysis, the p profiles were recorded along the illuminated lines. We find that the p values vary with N and have the highest value for the multilayer with the lowest N . Bilayer repetition dependence of AODF has been reported in earlier publications, and the less efficient switching for multilayers with higher bilayer repetitions (N) was attributed to the reduced domain size due to increasing

dipolar fields [13,20]. In agreement with earlier reports, our results in Figs. 5(a), 5(c), and 5(e) indicate a decrease of the domain size with increasing thickness, i.e., with the increasing N [38]. We propose that the laser fluence optimum to observe AOS and AODF is related to H_C (as well as T_C [39]) as schematically shown in Fig. 5(g).

C. Domain formation and relaxation mechanism

The above observations point to the optically induced *heating* to be the essential parameter affecting AOS. Therefore, in the next step we cooled the $[\text{Co/Pt}]_3$ multilayer in order to reduce the maximum temperature reached due to optically induced heating of the sample and to partially inhibit AOS and AODF processes. In addition, we increased the time interval between consecutive pulses by lowering the laser repetition rate, which allowed more efficient cooling of the sample during this period. In Figs. 6(a)–6(c) the horizontal direction (from the left to the right) represents an increase of the pulse-to-pulse time interval from 1 to 50 ms corresponding to laser pulse repetition frequencies from 1 kHz to 20 Hz. The vertical direction (from the top to the bottom) represents an increase of the number of laser pulses from 10^3 to 3×10^4 applied to one particular spot.

At 250 K [Fig. 6(a)] we observe a clear decrease of the optically induced spot size when tuning the laser pulse train towards lower repetition rates. In the extreme case, at 10^3 pulses with 50 ms pulse-to-pulse time interval (the top right position), the optically induced domains did not form at

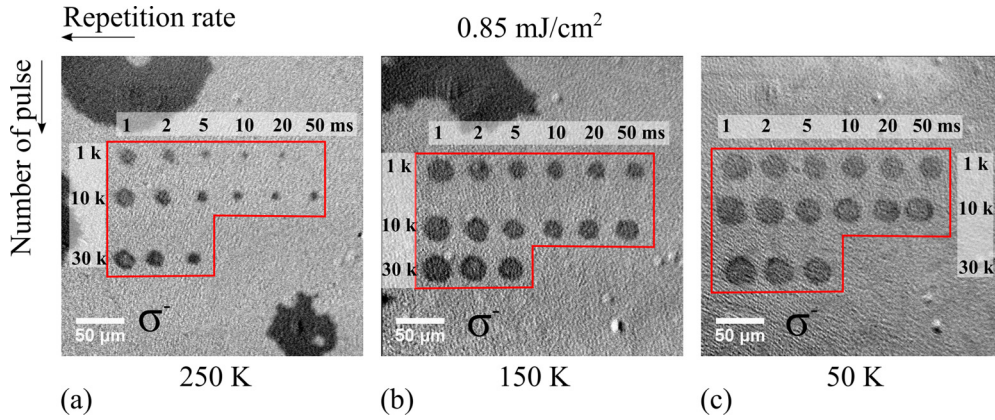


FIG. 6. Kerr microscopy images of a $[\text{Co}/\text{Pt}]_3$ multilayer at three different temperatures of (a) 250 K, (b) 150 K, and (c) 50 K. The laser repetition rate was varied from 1 to 0.02 kHz (corresponding pulse-to-pulse time intervals of 1 to 50 ms) in the horizontal direction. In addition, the number of pulses was kept constant in horizontal direction, but was varied along vertical direction from 10^3 to 3×10^4 .

all or their size was beyond the resolution limit. Since the average power, number of pulses, and the light polarization for every illuminated spot along the horizontal direction were kept constant, the observed changes are associated with the relaxation processes happening on the millisecond timescale.

Contrary to the measurement at 250 K, at lower temperatures, we observe, first, that all optically induced spots are nearly equal in size (particularly at 50 K) regardless of the laser repetition rate. Second, the diameters of these spots are substantially larger than the diameters of the spots illuminated at higher temperatures, although laser repetition rate and number of pulses per illuminated spot are the same. These observations are in contrast to the general expectation that a lower temperature reached by laser pulses should lead to a less efficient AOS/AODF and therefore should result in smaller spot sizes. These counterintuitive results indicate that the variation of the *ambient* temperature of the sample plays a minor role the formation of domains, although it decisively influence the relaxation process *after* the fs pulse illumination. These relaxation processes are more efficient at higher ambient temperature.

D. Discussions

In our quasidynamical domain formation and relaxation experiments, we controlled the sample temperature by tuning the time interval between the consecutive laser pulses. As a consequence, we observed a continuous drop in the spot diameter when the system was allowed to dissipate the temperature for a longer time from the illuminated area. This mechanism can be ascribed to thermal-gradient-driven domain wall (DW) motion from the cooler areas towards the hotter areas of the sample as suggested in theoretical calculations [40–42].

Immediately after the domain formation with the first single pulse, DWs drift towards the spot center considering that the temperature dissipation follows the Gaussian intensity profile. As a result, the larger time interval between the pulses results in formation of smaller spots, in agreement with our experimental observations. The time interval between the pulses allows a rough estimate of the DW speed. Assuming

that the spot of $\sim 15 \mu\text{m}$ radius [Fig. 6(c) top right] can collapse in 50 ms pulse-to-pulse time interval [Fig. 6(a) top right], the domain wall velocity is found to be of the order of 3×10^{-4} m/s.

Cooling the sample below room temperature results in a drop of the *ambient* temperature and rise of the sample coercivity H_C . One can therefore expect that a *larger* laser fluence would be required in order to reach the domain formation threshold that scales with the H_C of the sample in accordance with schematics shown in Fig. 5(g). Contrary to this expectation however, the optically induced spots at low temperatures are much *larger* compared to the spots illuminated at 250 K. At the same time, our experiments at low temperatures show that all the optically induced spots appear to have the same size regardless of the pulse-to-pulse interval. This observation is in agreement with the above discussed mechanism of the thermal gradient induced DW movement towards the spot center. We assume that a thermal gradient causes DW motion that proceeds via DW creep from one pinning center to another. If the ratio between activation energy to overcome the energy barrier of a pinning center and temperature, i.e., $\Delta E/k_B T$, increases at low temperatures, the thermal-gradient-driven DW motion stops, thus preventing the collapse of the optically induced spots and consequently results in larger spots.

Based on the above arguments, we propose a model involving three interlinked mechanisms: optically induced heating, magnetic circular dichroism (MCD), and the thermal-gradient-driven DW motion. In our physical picture, the laser pulse first heats up the magnetic system causing random domain formation with equally distributed up and down domains. Subsequent pulses further heat the system which results in a thermal gradient extending radially away from the hottest area at the center of the illuminated spot. A constant supply of heat maintains the AODF at the center of the spot. On the other hand, AOS forms at the perimeter of the illuminated area where the laser fluence at this part allows a MCD-driven helicity-dependent domain growth, see Fig. 5(h). In addition to the domain growth, domain walls experience a drift towards the center which in turn leads to a collapse of the

illuminated spots. We assume that the DW drift depends on the domain size and is less efficient for the larger domains because of the increased possibility of encountering more pinning centers. As the number of pulses impinging at the spot increases, the MCD-driven AOS regions are forming and the thermal-gradient flattens due to the lateral heat propagation. These evolving processes result in magnetic stabilization of the illuminated area due to the stronger pinning (larger domain walls) and smaller driving force (weaker thermal gradient).

Our experimental results in Fig. 5 can be better explained using the above physical picture. We observed a lower normalized domain contrast p in larger bilayer repetitions despite the fact that we illuminated the samples with minimum required laser fluence to influence magnetizations. The sample with larger intrinsic domains (as in [Co/Pt]₃ multilayer) display higher switching probability. In other words, larger domains in lower N multilayers that are formed by the first laser pulses can merge easier by the statistical process while smaller domains in higher N multilayers can collapse faster leading to incomplete switching for the same number of pulses. As discussed above, in case of circularly polarized pulses, the domain growth is ascribed to the MCD effect. This process is pursued with a number of pulses until the switched domains merge together to yield a complete switching.

To complete the physical picture, we interpret our results described in Sec. III B from a domain wall dynamics point of view. We first observed a decrease in p profiles with increasing laser fluence in the scanned lines (Fig. 3). This tendency can be attributed to the incomplete domain growth, because of the excessive heat given to the system. However, the helicity dependency is still maintained. Second, we observed an accumulative process in the onset of the “AOS ring” as well as an increased spot size with the increasing number of pulses (Fig. 4). The latter is intuitively ascribed to the radial propagation of the thermal gradient due to a constant heating by the set of laser pulses. Therefore, the optimum level of the optically induced heating as well drifts radially outwards.

IV. CONCLUSIONS

Our analysis show that the optically induced all-optical magnetization switching in [Co/Pt]_{*N*} multilayers is a consequence of multiple pulse accumulation, and it involves material heating, magnetic circular dichroism, as well as the thermal-gradient-driven domain wall motion mechanisms. In our physical picture, first, the laser pulse heats up the material causing a randomly distributed multidomain state. Optically induced magnetic domains rapidly move towards the spot center, whereas the subsequent pulses provide an optimum heating level for helicity-dependent domain growth due to the broken magnetic symmetry via magnetic circular dichroism. Nevertheless, the role of the inverse Faraday effect as a contribution to the symmetry breaking of the switching process requires further investigation.

All-optical switching (AOS) efficiency is expected to be higher for materials with larger domains, since the individual domains can merge and to become more resistant against the collapse under thermal gradient. This argument is supported by the AOS experiments on the multilayers where the sample coercivity and the domain size are tuned. As the number of pulses impinging at the spot increases, the thermal-gradient flattens due to lateral heat propagation and leads to a stabilized magnetic domain state due to the stronger pinning and smaller driving force.

The above physical picture points to the importance of the domain relaxation dynamics and the material properties affecting the magnetic domain size. We believe that our analysis will contribute to the understanding of the laser-induced switching process and the further optimization of the optically switchable magnetic materials.

ACKNOWLEDGMENT

The authors gratefully acknowledge S. Nemšák and T. Duchoň for the acquisition of PEEM images shown in the Supplemental Material [36].

-
- [1] E. Beaurepaire, J.-C. Merle, A. Daunois, and J.-Y. Bigot, *Phys. Rev. Lett.* **76**, 4250 (1996).
 - [2] E. Beaurepaire, M. Maret, V. Halté, J.-C. Merle, A. Daunois, and J.-Y. Bigot, *Phys. Rev. B* **58**, 12134 (1998).
 - [3] J. Hohlfeld, T. Gerrits, M. Bilderbeek, T. Rasing, H. Awano, and N. Ohta, *Phys. Rev. B* **65**, 012413 (2001).
 - [4] B. Koopmans, M. Van Kampen, and W. De Jonge, *J. Phys.: Condens. Matter* **15**, S723 (2003).
 - [5] C. D. Stanciu, F. Hansteen, A. V. Kimel, A. Kirilyuk, A. Tsukamoto, A. Itoh, and Th. Rasing, *Phys. Rev. Lett.* **99**, 047601 (2007).
 - [6] S. Alebrand, M. Gottwald, M. Hehn, D. Steil, M. Cinchetti, D. Lacour, E. E. Fullerton, M. Aeschlimann, and S. Mangin, *Appl. Phys. Lett.* **101**, 162408 (2012).
 - [7] A. Hassdenteufel, B. Hebler, C. Schubert, A. Liebig, M. Teich, M. Helm, M. Aeschlimann, M. Albrecht, and R. Bratschitsch, *Adv. Mater.* **25**, 3122 (2013).
 - [8] S. Mangin, M. Gottwald, C. Lambert, D. Steil, V. Uhlíř, L. Pang, M. Hehn, S. Alebrand, M. Cinchetti, G. Malinowski *et al.*, *Nat. Mater.* **13**, 286 (2014).
 - [9] A. Hassdenteufel, J. Schmidt, C. Schubert, B. Hebler, M. Helm, M. Albrecht, and R. Bratschitsch, *Phys. Rev. B* **91**, 104431 (2015).
 - [10] I. Radu, K. Vahaplar, C. Stamm, T. Kachel, N. Pontius, H. Dürr, T. Ostler, J. Barker, R. Evans, R. Chantrell *et al.*, *Nature (London)* **472**, 205 (2011).
 - [11] T. Ostler, J. Barker, R. Evans, R. Chantrell, U. Atxitia, O. Chubykalo-Fesenko, S. El Moussaoui, L. Le Guyader, E. Mengotti, L. Heyderman *et al.*, *Nat. Commun.* **3**, 666 (2012).
 - [12] M. S. El Hadri, M. Hehn, G. Malinowski, and S. Mangin, *J. Phys. D* **50**, 133002 (2017).
 - [13] C.-H. Lambert, S. Mangin, B. C. S. Varaprasad, Y. Takahashi, M. Hehn, M. Cinchetti, G. Malinowski, K. Hono, Y. Fainman, M. Aeschlimann *et al.*, *Science* **345**, 1337 (2014).
 - [14] Y. K. Takahashi, R. Medapalli, S. Kasai, J. Wang, K. Ishioka, S. H. Wee, O. Hellwig, K. Hono, and E. E. Fullerton, *Phys. Rev. Appl.* **6**, 054004 (2016).
 - [15] R. John, M. Berritta, D. Hinzke, C. Müller, T. Santos, H. Ulrichs, P. Nieves, J. Walowski, R. Mondal, O. Chubykalo-Fesenko *et al.*, *Sci. Rep.* **7**, 4114 (2017).

- [16] F. Hellman, A. Hoffmann, Y. Tserkovnyak, G. S. Beach, E. E. Fullerton, C. Leighton, A. H. MacDonald, D. C. Ralph, D. A. Arena, H. A. Dürr *et al.*, *Rev. Mod. Phys.* **89**, 025006 (2017).
- [17] J. Gorchon, Y. Yang, and J. Bokor, *Phys. Rev. B* **94**, 020409 (2016).
- [18] T. Cornelissen, R. Córdoba, and B. Koopmans, *Appl. Phys. Lett.* **108**, 142405 (2016).
- [19] R. Medapalli, D. Afanasiev, D. K. Kim, Y. Quessab, S. Manna, S. A. Montoya, A. Kirilyuk, Th. Rasing, A. V. Kimel, and E. E. Fullerton, *Phys. Rev. B* **96**, 224421 (2017).
- [20] M. S. El Hadri, P. Pirro, C.-H. Lambert, S. Petit-Watelot, Y. Quessab, M. Hehn, F. Montaigne, G. Malinowski, and S. Mangin, *Phys. Rev. B* **94**, 064412 (2016).
- [21] A. R. Khorsand, M. Savoini, A. Kirilyuk, A. V. Kimel, A. Tsukamoto, A. Itoh, and Th. Rasing, *Phys. Rev. Lett.* **108**, 127205 (2012).
- [22] M. O. Ellis, E. E. Fullerton, and R. W. Chantrell, *Sci. Rep.* **6**, 30522 (2016).
- [23] K. Vahaplar, A. M. Kalashnikova, A. V. Kimel, D. Hinzke, U. Nowak, R. Chantrell, A. Tsukamoto, A. Itoh, A. Kirilyuk, and Th. Rasing, *Phys. Rev. Lett.* **103**, 117201 (2009).
- [24] A. Kirilyuk, A. V. Kimel, and T. Rasing, *Rev. Mod. Phys.* **82**, 2731 (2010).
- [25] G. Zhang, T. Latta, Z. Babyak, Y. Bai, and T. F. George, *Mod. Phys. Lett. B* **30**, 16300052 (2016).
- [26] M. Berritta, R. Mondal, K. Carva, and P. M. Oppeneer, *Phys. Rev. Lett.* **117**, 137203 (2016).
- [27] M. L. M. Laliou, M. J. G. Peeters, S. R. R. Haenen, R. Lavrijsen, and B. Koopmans, *Phys. Rev. B* **96**, 220411(R) (2017).
- [28] J. Gorchon, C.-H. Lambert, Y. Yang, A. Pattabi, R. B. Wilson, S. Salahuddin, and J. Bokor, *Appl. Phys. Lett.* **111**, 042401 (2017).
- [29] M. Vomir, M. Albrecht, and J.-Y. Bigot, *Appl. Phys. Lett.* **111**, 242404 (2017).
- [30] J.-H. Kim and S.-C. Shin, *J. Appl. Phys.* **80**, 3121 (1996).
- [31] W. Zeper, H. Van Kesteren, B. Jacobs, J. Spruit, and P. Carcia, *J. Appl. Phys.* **70**, 2264 (1991).
- [32] G. Zhang, Y. Bai, and T. F. George, *J. Phys.: Condens. Matter* **29**, 425801 (2017).
- [33] T. Suzuki, H. Notarys, D. Dobbertin, C.-J. Lin, D. Weller, D. Müller, and G. Gorman, *IEEE Trans. Magn.* **28**, 2754 (1992).
- [34] D. Weller, H. Notarys, T. Suzuki, G. Gorman, T. Logan, I. McFadyen, and C. Chien, *IEEE Trans. Magn.* **28**, 2500 (1992).
- [35] J. W. Knepper and F. Y. Yang, *Phys. Rev. B* **71**, 224403 (2005).
- [36] See Supplemental Material at <http://link.aps.org/supplemental/10.1103/PhysRevB.98.214443> for brief description of magnetic domain images obtained by PEEM, and the domain contrast profiles.
- [37] S. Alebrand, A. Hassdenteufel, D. Steil, M. Cinchetti, and M. Aeschlimann, *Phys. Rev. B* **85**, 092401 (2012).
- [38] O. Hellwig, A. Berger, J. B. Kortright, and E. E. Fullerton, *J. Magn. Magn. Mater.* **319**, 13 (2007).
- [39] P. G. Pitcher, J. Miller, D. P. A. Pearson, and P. D. Gurney, *J. Magn. Soc. Jpn.* **17**, 95 (1993).
- [40] J. Chico, C. Etz, L. Bergqvist, O. Eriksson, J. Fransson, A. Delin, and A. Bergman, *Phys. Rev. B* **90**, 014434 (2014).
- [41] S. Moretti, V. Raposo, E. Martinez, and L. Lopez-Diaz, *Phys. Rev. B* **95**, 064419 (2017).
- [42] F. Schlickeiser, U. Ritzmann, D. Hinzke, and U. Nowak, *Phys. Rev. Lett.* **113**, 097201 (2014).